
Article:
Takeshita, S, Sadeghpour, A orcid.org/0000-0002-0475-7858, Malfait, WJ et al. (3 more authors) (2019) Formation of Nanofibrous Structure in Biopolymer Aerogel during Supercritical CO2 Processing: The Case of Chitosan Aerogel. Biomacromolecules, 20 (5). pp. 2051-2057. ISSN 1525-7797

https://doi.org/10.1021/acs.biomac.9b00246

Formation of Nanofibrous Structure in Biopolymer Aerogel during Supercritical CO_2 Processing: The Case of Chitosan Aerogel

Satoru Takeshita,*,† Amin Sadeghpour,‡ Wim J. Malfait,§ Arata Konishi,⊥ Katsuto Otake,⊥ and Satoshi Yoda†

†Research Institute for Chemical Process Technology, National Institute of Advanced Industrial Science and Technology (AIST), Tsukuba 3058565, Japan

‡Center for X-ray Analytics, Department of Materials Meet Life, Empa, Swiss Federal Laboratories for Materials Science and Technology, St. Gallen CH-9014, Switzerland

§Laboratory for Building Energy Materials and Components, Empa, Swiss Federal Laboratories for Materials Science and Technology, Dübendorf CH-8600, Switzerland

⊥Department of Industrial Chemistry, Tokyo University of Science, Tokyo 1628601, Japan

Biopolymer aerogels are open-celled, predominantly mesoporous solids of natural and seminatural polymers typically produced by supercritical drying. The first biopolymer aerogels were reported as early as the 1930s,[1] but in the last decade, they have become a remarkably hot topic in material science after the industrial success of silica-based aerogels and in the search for more sustainable precursors.[2−4] Biopolymers have suitable properties for the sustainable chemistry today, e.g., biocompatibility, abundant resources, low environmental loads, and flexibility for functionalization. Connecting the inherent advantages of biopolymers with the three-dimensional unique structures of aerogels has opened up attractive new potential applications in flexible thermal superinsulation,[3,4] biomedical scaffolds,[3,4] energy storage devices,[5] drug carriers,[6] catalysts,[7] and food processing.[8] However, the clarification of the potential of the materials still requires more fundamental scientific insights into the synthetic processes, structures, and properties of biopolymer aerogels. The present work provides an important mechanism for biopolymer aerogel structure formation that has not been recognized to date and may overturn, or at least expand, the conventional concept of supercritical drying.

The field of aerogels started by the realization by Kistler in 1931 that the liquid in a jelly can be replaced by a gas without shrinkage through the use of a supercritical fluid.[1] Since then, supercritical drying has been established as the standard method of preparing aerogels, both for academic and industrial production. The current paradigm states that supercritical drying preserves the inner microstructure of the wet gel because of the absence of liquid–gas interfaces.[9] In fact, Kistler's initial goal in preparing aerogels was to open new investigative opportunities into the structure of gels, and this is still an important line of aerogel research today. Since then, numerous studies investigated microstructure formation inside wet gels. For silica aerogels, the picture is clear: preformed, primary silica nanoparticles in the sol interconnect to construct a three-dimensional nanoparticulate skeleton, most often in response to a change in pH.[10,11] The gelation of biopolymer aerogels from nanofibrillated building blocks can proceed along a similar vein, i.e., the pH-triggered gelation of nanofibrillated cellulose[12,13] and chitin nanofibers.[14] In contrast, structure formation is more complex for polymer aerogels from molecular precursors, e.g., fully dissolved polymer chains of chitosan, pectin, alginate, and cellulose, and this is the focus of this study.

Gels from molecular precursors can be prepared via physical processes, including pH-triggered regeneration from fully dissolved chitosan,[14,15] starch,[17] and cellulose solutions,[18] antisolvent precipitation of chitin,[19] cellulose,[18,20,21] and other polysaccharides,[22] ion-exchange-triggered gelation of cellulose–alkaline hydroxide solution,[23] regeneration from ionic liquid solutions,[24,25] and temperature-induced gelation.[26−28] Physical cross-linking by adding electrostatic cross-linkers is possible for molecular precursors of alginate,[29] pectin,[30] and chitosan.[31] Finally, chemical cross-linking forms covalent molecular network gels such as cross-linked chitosan,[32−35] xanthan,[36] and galactomannan.[37] Sometimes phase separation is responsible for micrometer-scale structures,[20,28,38] and very recently, spinodal decomposition was also proposed to explain the nanoscale concentration contrast formation.[39]

In the vast majority of these studies, the structure formation is assumed to occur during gelation, with at most minor modifications during subsequent processing, including supercritical drying. However, this has not been shown experimentally in most biopolymer systems. Here, we investigate the formation of a nanofibril-like microstructure in chitosan aerogel.[33] We provide tantalizing evidence that the post-gelation treatment of the hydro-

gels, and the solvent exchange with CO_2 at the first step of supercritical drying process in particular, is the key step in forming the nanofibrous aerogel structure.

The chitosan aerogel was prepared by chemical cross-linking gelation with formaldehyde, followed by solvent exchange with methanol and supercritical drying using CO_2 (see SI for the detailed procedure). The chitosan aerogel consists of three-dimensionally entangled nanofibers with a diameter of approximately 5–30 nm (Fig. 1). Assuming that one chitosan molecule occupies 0.4 nm² in the cross section,[35,40] each nanofiber would consist of 50–1800 molecules. The individual nanofibers are not well-separated or stretched, instead, they form some particle-like aggregates and branched networks (Fig. S1). In contrast to the aerogel, no trace of nanofibrous or nanoparticulate structures is observed for the xerogel, which are transparent films with a completely smooth surface at the nanoscale (Figs. 1 and S2). Freeze-dried cryogels display a secondary macroporosity due to ice crystal growth and the chitosan sheets that separate the pores are completely smooth surface at the nanoscale (Figs. S4 and S5).

The XRD profiles (Fig. S6) show that the starting chitosan reagent consists of partially crystalline microfibrils as it was produced from chitin of natural crab shells. The gels however are fully amorphous. This means the microfibrillar structure of the chitosan flakes is destroyed at the molecular level upon dissolution in acetic acid, and new structures are built up again during the subsequent steps as amorphous chitosan. Considering the widely accepted concepts of structure formation in aerogels, one would assume that the nanofibrous structure observed in the aerogel is formed along with the gelation and retained by supercritical drying. The lack of nanoscale features for the xerogels and cryogels would be assumed to be the result of structural degradation during ambient pressure and freeze dryings, respectively. However, the small angle X-ray scattering (SAXS) analysis has revealed a different mechanism in the present case.

The SAXS profile (Fig. 2a) of the starting chitosan solution displays a broad correlation peak at q ~0.5 nm⁻¹, consistent with the previous literature.[41] After the cross-linking, this correlation peak disappears, and the hydrogel as well as the organogel show roughly linear profiles with a decaying slope of ~1.4 in the q > 0.2 nm⁻¹ region in the log–log plots. On the other hand, the profile of the aerogel consists of two regions with a slope of ~4 for q > 0.6 nm⁻¹ and ~1.6 for q < 0.6 nm⁻¹, similar to those of nanofibrous cellulose aerogel[25] and to those of nanofibrous wet gels prepared mainly by physical coagulation.[23,42,43]

The Kratky plots (Fig. 2b), intensity × q² vs q, demonstrate clear differences between the polymer chain configurations, i.e., swollen, Gaussian, and collapsed chains. The starting chitosan solution exhibits an monotonous increasing behavior towards higher q values, which is an indication of swollen chains with linear expansion.[44] The scattering profile was further considered for modelling

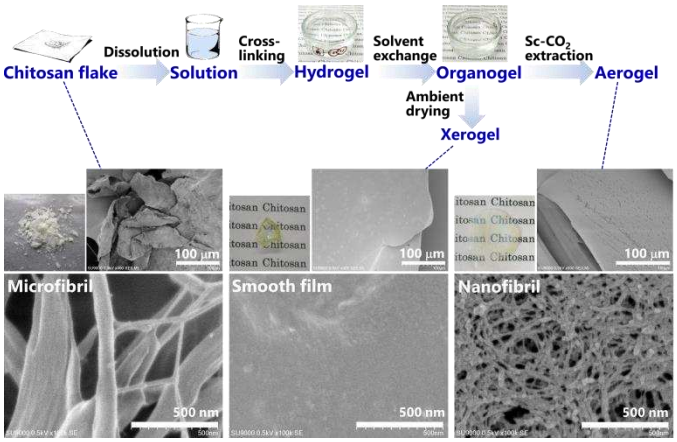

Figure 1. Aerogel production scheme and SEM images (see Figs. S1–S5 for additional SEM images).

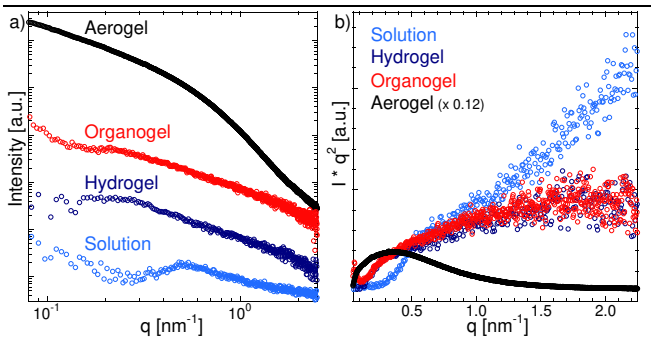

Figure 2. SAXS (a) and Kratky (b) profiles for different steps in the aerogel production.

with a function composed of Porod and a correlation peak function, resulting in a correlation length of 4.4 nm (Fig. S7, see SAXS fitting details in SI).[41,45] The Kratky plots of hydrogel and organogel mainly show Gaussian chain behavior, i.e. ideal or random walk chains equivalent to the polymers in good solvents. Noteworthy that, the upturn at low q values also could be a signature of a minor amounts of collapsed chains. The fitting analysis gives a radius of gyration, R_g, of 4–5 nm for both wet gels (Fig. S8). In contrast, the Kratky plot of the aerogel shows a maximum followed by a decrease and a plateau at high q. This downward deviation from the Debye function indicates a mass fractal configuration of aggregated polymer chains, which reflects the microstructure observed in SEM. The R_g value is estimated at 18.2 nm (Fig. S9). We also implemented an indirect Fourier transform approach to fit the whole curve of the aerogel,[46,47] where the scattering intensity is mainly assumed to originate from the high contrast between polymer aggregates and the voids. This approach gives a polydispersed aggregates structure with R_g = 17.4 nm (Fig. S10), which is in good agreement with Kratky analysis. In summary, the SAXS data demonstrate that the hydrogel and organogel are simple chemically cross-linked molecular gels without a rigid structure of well-separated polymer/solvent phases. We therefore conclude that the nanofibrous structure of the aerogel is formed during the processing steps between organogel and aerogel, i.e., during supercritical drying.

The microstructure formation during supercritical processing correlates with volumetric changes of the gel. In contrast to silica-based gels, the cross-linked chitosan gel shows a dynamic change in size without breaking.[48,49] For example, the as-prepared hydrogel first expands by ~30% in methanol and then shrinks back by ~15% as the solvent exchange proceeds (Fig. S11). *In situ* observations during supercritical drying reveal that the most drastic change occurs in the initial steps of supercritical CO_2 processing: the thickness of the organogel is reduced by half, corresponding to a 80–90% reduction in volume in an assumption of isotropic shrinkage, during heating and CO_2 introduction (Fig. 3a). Since the subsequent extraction and decompression do not affect the gel size, either the solvent exchange from methanol to liquid/supercritical CO_2 or the increase in temperature must be the main cause this volumetric change. To distinguish between both causes, we introduced liquid CO_2 at ~6.4 MPa without heating. As shown in Figs. 3b,c and S12, the gel also shrinks in liquid CO_2, and the shrinkage is more drastic with a larger fraction of CO_2. These results prove that the volumetric change is caused by solvent exchange from methanol to CO_2, and not by the increase in pressure or temperature.

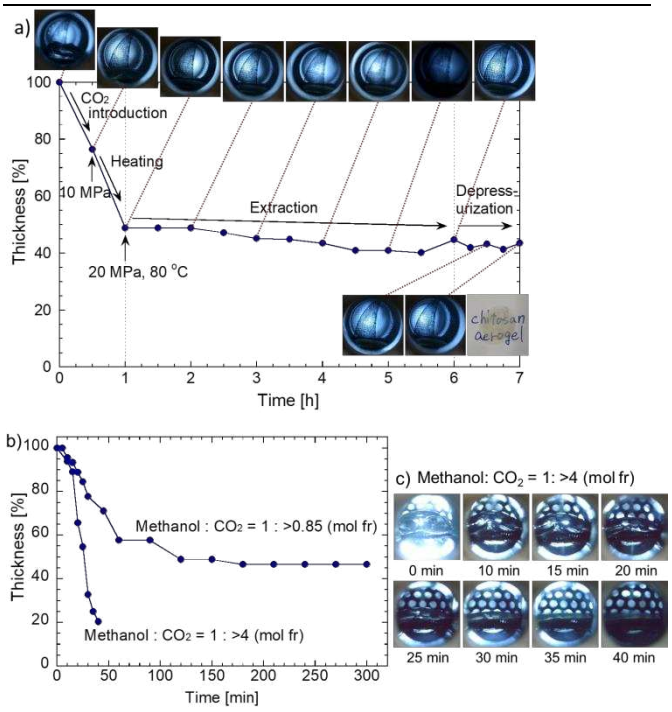

Figure 3. Change in gel thickness with time (a) during the supercritical drying and (b,c) in liquid CO_2 at 25 °C and ~6.4 MPa. (c) Pictures of gel in methanol:CO_2 = 1: >4 (mol fr) (see Fig. S12 for methanol:CO_2 = 1: >0.85).

We suggest that the affinity between chitosan and solvents plays a significant role to trigger the shrinkage and structure formation. The Flory–Huggins interaction parameter, χ, which can be estimated from solubility parameters, represents the affinity between a solvent and a polymer:[50]

$$\chi = \frac{V\{(\delta_{d1}-\delta_{d2})^2+0.25(\delta_{p1}-\delta_{p2})^2+0.25(\delta_{h1}-\delta_{h2})^2\}}{RT} \quad (1)$$

where δ_{d1}, δ_{p1}, δ_{h1} and δ_{d2}, δ_{p2}, δ_{h2} are the Hansen solubility parameters for dispersion, polarity, and hydrogen bonding of the solvent and solute, respectively, R is the gas constant, T is the temperature, and V is the molar volume of the solvent (Table S1). Molecular chitosan has a large contribution from hydrogen bonding because of the OH and NH_2 groups.[51,52] Hence, it has high affinity with hydrating solvents such as water and methanol. The χ values between molecular chitosan and solvents are calculated to be water (0.85) < methanol (1.15) << supercritical CO_2 (~11) < liquid CO_2 (~60), where larger values mean less affinity. Although the actual chitosan in this study is not simply molecular chitosan but a cross-linked chitosan gel, these values provide a qualitative explanation for the shrinkage and structure formation behavior.

Based on all the observations, we propose the following mechanism for the nanofibrous structure formation (Fig. 4). As the fraction of CO_2 introduced into the gel increases, the low affinity between chitosan and CO_2 causes the macroscopic shrinkage and the coagulation between individual chains. The coagulated polymers are held together by hydrogen bonds to form nanofibers and nanoparticle-like aggregates, which magnifies the inhomogeneous density distribution in the wet gel. This newly formed microstructure is then retained in the aerogel because of the absence of surface tensions during the depressurization process.

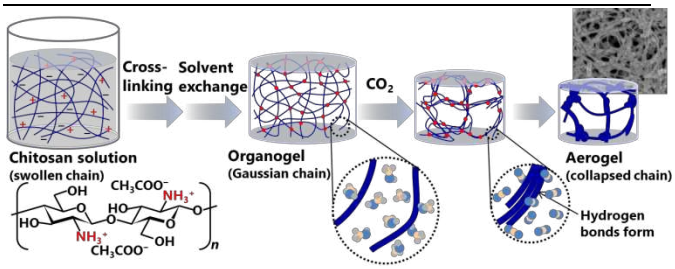

Figure 4. Proposed mechanism for nanofibrous structure formation in CO_2. Images are not to scale.

In conclusion, we have found a new aspect that expands the conventional idea of supercritical drying: CO_2 processing as a microstructure forming step. The SAXS analysis and *in situ* observation of the gel volume reveal that the nanofibrous network structure of the chitosan aerogel forms during the CO_2 processing, most likely through the physical coagulation of chitosan chains in CO_2. Note that the structural and volumetric changes during supercritical drying are not necessarily detrimental to the final aerogel properties. In fact, in the case of the chitosan aerogels studied here, it is the nanofibrous structure formed during CO_2 processing that imparts the aerogels with their excellent optical and mechanical properties and ultralow thermal conductivity.[49] Finally, large volumetric changes during supercritical drying are not a phenomenon unique to chitosan, but a general feature of (bio)polymer aerogel production, including polyurethane,[53] alginate,[54] and regenerated cellulose aerogels.[55]

Thus, structure formation during CO_2 processing may be important for many other polysaccharide, biopolymer, and polymer aerogel systems and, when understood completely and utilized intelligently, may enable the production of even higher performing materials.

ASSOCIATED CONTENT

Supporting Information. Experimental details, SEM images, XRD profiles, SAXS fitting details, change in gel size, solubility parameters. This material is available free of charge via the Internet at http://pubs.acs.org.

AUTHOR INFORMATION

Corresponding Author

*s.takeshita@aist.go.jp

Author Contributions

The manuscript was written through contributions of all authors. All authors have given approval to the final version of the manuscript.

Funding Sources

This work was supported by JSPS KAKENHI Grant Number JP16K17491.

Notes

The cross-linked chitosan aerogel is the subject of a Japanese patent application by AIST.

REFERENCES

(1) Kistler, S. S. Coherent Expanded Aerogels and Jellies. *Nature* **1931**, *127*, 741.

(2) Aegerter, M.; Leventis, N.; Koebel, M. M. ed. *Aerogels Handbook*, Springer, New York, 2011.

(3) Zhao, S.; Malfait, W. J.; Alburquerque, N. G.; Koebel, M. M.; Nyström, G. Biopolymer Aerogels and Foams: Chemistry, Properties, and Applications. *Angew. Chem. Int. Ed.* **2018**, *57*, 7580–7608.

(4) Lavoine, N.; Bergström, L. Nanocellulose-based foams and aerogels: processing, properties, and applications. *J. Mater. Chem. A* **2017**, *5*, 16105–16117.

(5) De France, K. J.; Hoare, T.; Cranston, E. D. Review of Hydrogels and Aerogels Containing Nanocellulose. *Chem. Mater.* **2017**, *29*, 4609–4631.

(6) García-González, C. A.; Alnaief, M.; Smirnova, I. Polysaccharide-based aerogels—Promising biodegradable carriers for drug delivery systems. *Carbohydr. Polym.* **2011**, *86*, 1425–1438.

(7) Quignard, F.; Valentin, R.; Di Renzo, F. Aerogel materials from marine polysaccharides. *New J. Chem.* **2008**, *32*, 1300–1310.

(8) Mikkonen, K. S.; Parikka, K.; Ghafar, A.; Tenkanen, M. Prospects of polysaccharide aerogels as modern advanced food materials. *Trends Food Sci. Technol.* **2013**, *34*, 124–136.

(9) Smirnova, I.; Gurikov, P. Aerogel production: Current status, research directions, and future opportunities. *J. Supercrit. Fluids* **2018**, *134*, 228–233.

(10) Hüsing, N.; Schubert, U. Aerogels—Airy Materials: Chemistry, Structure, and Properties. *Angew. Chem. Int. Ed.* **1998**, *37*, 22–45.

(11) Pierre, A. C.; Pajonk, G. M. Chemistry of Aerogels and Their Applications. *Chem. Rev.* **2002**, *102*, 4243–4266.

(12) Kobayashi, Y.; Saito, T.; Isogai, A. Aerogels with 3D Ordered Nanofiber Skeletons of Liquid-Crystalline Nanocellulose Derivatives as Tough and Transparent Insulators. *Angew. Chem. Int. Ed.* **2014**, *53*, 10394–10397.

(13) Plappert, S. F.; Nedelec, J.-M.; Rennhofer, H.; Lichtenegger, H. C.; Liebner, F. W. Strain Hardening and Pore Size Harmonization by Uniaxial Densification: A Facile Approach toward Superinsulating Aerogels from Nematic Nanofibrillated 2,3-Dicarboxyl Cellulose. *Chem. Mater.* **2017**, *29*, 6630–6641.

(14) Ding, B.; Huang, S.; Pang, K.; Duan, Y.; Zhang, J. Nitrogen-Enriched Carbon Nanofiber Aerogels Derived from Marine Chitin for Energy Storage and Environmental Remediation. *ACS Sustainable Chem. Eng.* **2018**, *6*, 177–185.

(15) Valentin, R.; Bonelli, B.; Garrone, E.; Di Renzo, F.; Quignard, F. Accessibility of the Functional Groups of Chitosan Aerogel Probed by FT-IR-Monitored Deuteration. *Biomacromol.* **2007**, *8*, 3646–3650.

(16) Ricci, A.; Bernardi, L.; Gioia, C.; Vierucci, S.; Robitzer, M.; Quignard, F. Chitosan aerogel: a recyclable, heterogeneous organocatalyst for the asymmetric direct aldol reaction in water. *Chem. Commun.* **2010**, *46*, 6288–6290.

(17) Kenar, J. A.; Eller, F. J.; Felker, F. C.; Jackson, M. A.; Fanta, G. F. Starch aerogel beads obtained from inclusion complexes prepared from high amylose starch and sodium palmitate. *Green Chem.* **2014**, *16*, 1921–1930.

(18) Cai, J.; Kimura, S.; Wada, M.; Kuga, S.; Zhang, L. Cellulose Aerogels from Aqueous Alkali Hydroxide–Urea Solution. *ChemSusChem* **2008**, *1*, 149–151.

(19) Ding, B.; Cai, J.; Huang, J.; Zhang, L.; Chen, Y.; Shi, X.; Du, Y.; Kuga, S. Facile preparation of robust and biocompatible chitin aerogels. *J. Mater. Chem.* **2012**, *22*, 5801–5809.

(20) Pour, G.; Beauger, C.; Rigacci, A.; Budtova, T. Xerocellulose: lightweight, porous and hydrophobic cellulose prepared via ambient drying. *J. Mater. Sci.* **2015**, *50*, 4526–4535.

(21) Schestakow, M.; Karadagli, I.; Ratke, L. Cellulose aerogels prepared from an aqueous zinc chloride salt hydrate melt. *Carbohydr. Polym.* **2016**, *137*, 642–649.

(22) Tkalec, G.; Knez, Ž.; Novak, Z. Formation of polysaccharide aerogels in ethanol. *RSC Adv.* **2015**, *5*, 77362–77371.

(23) Ishii, D.; Tatsumi, D.; Matsumoto, T.; Murata, K.; Hayashi, H.; Yoshitani, H. Investigation of the Structure of Cellulose in LiCl/DMAc Solution and Its Gelation Behavior by Small-Angle X-Ray Scattering Measurements. *Macromol. Biosci.* **2006**, *6*, 293–300.

(24) Shen, X.; Shamshina, J. L.; Berton, P.; Bandomir, J.; Wang, H.; Gurau, G.; Rogers, R. D. Comparison of Hydrogels Prepared with Ionic-Liquid-Isolated vs Commercial Chitin and Cellulose. *ACS Sustainable Chem. Eng.* **2018**, *4*, 471–480.

(25) Plappert, S. F.; Nedelec, J.-M.; Rennhofer, H.; Lichtenegger, H. C.; Bernstorff, S.; Liebner, F. W. Self-Assembly of Cellulose in Super-Cooled Ionic Liquid under the Impact of Decelerated Antisolvent Infusion: An Approach toward Anisotropic Gels and Aerogels. *Biomacromol.* **2018**, *11*, 4411–4422.

(26) García-González, C. A.; Smirnova, I. Use of supercritical fluid technology for the production of tailor-made aerogel particles for delivery systems. *J. Supercrit. Fluids* **2013**, *79*, 152–158.

(27) Druel, L.; Bardl, R.; Vorwerg, W.; Budtova, T. Starch Aerogels: A Member of the Family of Thermal Superinsulating Materials. *Biomacromol.* **2017**, *18*, 4232–4239.

(28) Gavillon, R.; Budtova, T. Aerocellulose: New Highly Porous Cellulose Prepared from Cellulose–NaOH Aqueous Solutions. *Biomacromol.* **2008**, *9*, 269–277.

(29) Robitzer, M.; David, L.; Rochas, C.; Di Renzo, F.; Quignard, F. Nanostructure of Calcium Alginate Aerogels Obtained from Multistep Solvent Exchange Route. *Langmuir* **2008**, *24*, 12547–12552.

(30) Groult, S.; Budtova, T. Thermal conductivity/structure correlations in thermal super-insulating pectin aerogels. *Carbohydr. Polym.* **2018**, *196*, 73–81.

(31) Obaidat, R. M.; Tashtoush, B. M.; Bayan, M. F.; Al Bustami, R. T.; Alnaief, M. Drying Using Supercritical Fluid

Technology as a Potential Method for Preparation of Chitosan Aerogel Microparticles. *AAPS PharmSciTech* **2015**, *16*, 1235–1244.

(32) Rinki, K.; Dutta, P. K.; Hunt, A. J.; Macquarrie, D. J.; Clark, J. H. Chitosan Aerogels Exhibiting High Surface Area for Biomedical Application: Preparation, Characterization, and Antibacterial Study. *Int. J. Polym. Mater.* **2011**, *60*, 988–999.

(33) Takeshita, S.; Yoda, S. Chitosan Aerogels: Transparent, Flexible Thermal Insulators. *Chem. Mater.* **2015**, *27*, 7569–7572.

(34) Takeshita, S.; Konishi, A.; Takebayashi, Y.; Yoda, S.; Otake, K. Aldehyde Approach to Hydrophobic Modification of Chitosan Aerogels. *Biomacromol.* **2017**, *18*, 2172–2178.

(35) Takeshita, S.; Yoda, S. Translucent, hydrophobic, and mechanically tough aerogels constructed from trimethylsilylated chitosan nanofibers. *Nanoscale* **2017**, *9*, 12311–12315.

(36) Bilanovic, D.; Starosvetsky, J.; Armon, R. H. Preparation of Biodegradable Xanthan–Glycerol Hydrogel, Foam, Film, Aerogel and Xerogel at Room Temperature. *Carbohydr. Polym.* **2016**, *148*, 243–250.

(37) Ghafar, A.; Gurikov, P.; Subrahmanyam, R.; Parikka, K.; Tenkanen, M.; Smirnova, I.; Mikkonen, K. S. Mesoporous guar galactomannan based biocomposite aerogels through enzymatic crosslinking. *Compos. A: Appl. Sci. Manufact.* **2017**, *94*, 93–103.

(38) Pircher, N.; Carbajal, L.; Schimper, C.; Bacher, M.; Rennhofer, H.; Nedelec, J.-M.; Lichtenegger, H. C.; Rosenau, T.; Liebner, F. Impact of selected solvent systems on the pore and solid structure of cellulose aerogels. *Cellulose* **2016**, *23*, 1949–1966.

(39) Ratke, L.; Wang, F.; Nestler, B. Polymerization induced phase separation – a mechanism for structure formation in aerogels? *Proceedings of the 4th International Seminar on Aerogels,* 2018, p.66.

(40) Naito, P.-K.; Ogawa, Y.; Sawada, D.; Nishiyama, Y.; Iwata, T.; Wada, M. X-ray Crystal Structure of Anhydrous Chitosan at Atomic Resolution. *Biopolymers* **2016**, *105*, 361–368.

(41) David, L.; Montembault, A.; Vizio, N. G.; Crepet, A.; Viton, C.; Domard, A.; Morfin, I.; Rochas, C. Ordering in biopolyelectrolyte chitosan solutions. *Macromol. Symp.* **2005**, *222*, 281–286.

(42) Jeong, Y.; Friggeri, A.; Akiba, I.; Masunaga, H.; Sakurai, K.; Sakurai, S.; Okamoto, S.; Inoue, K.; Shinkai, S. Small-angle X-ray scattering from a dual-component organogel to exhibit a charge transfer interaction. *J. Colloid Interface Sci.* **2008**, *283*, 113–122.

(43) Leppänen, K.; Pirkkalainen, K.; Penttilä, P.; Sievänen, J.; Kotelnikova, N.; Serimaa, R. Small-angle x-ray scattering study on the structure of microcrystalline and nanofibrillated cellulose. *J. Phys.: Conf. Ser.* **2010**, *247*, 012030.

(44) Benoit, H.; Joanny, J. F.; Hadziioannou, G.; Hammouda, B. Scattering by linear, branched, and copolymer chain molecules for large scattering vectors. *Macromolecules* **1993**, *26*, 5790–5795.

(45) Hammouda, B.; Ho, D. L.; Kline, S. Insight into Clustering in Poly(ethylene oxide) Solutions. *Macromolecules* **2004**, *37*, 6932–6937.

(46) Glatter, O. Chapter 3 - The Inverse Scattering Problem, *Scattering Methods and their Application in Colloid and Interface Science*, Elsevier, 2018, pp. 33–74.

(47) Glatter, O. A New Method for the Evaluation of Small-Angle Scattering Data. *J. Appl. Crystallogr.* **1977**, *10*, 415–421.

(48) Takeshita, S.; Takebayashi, Y.; Nakamura, H.; Yoda, S. Gas-Responsive Photoluminescence of YVO_4:Eu^{3+} Nanoparticles Dispersed in an Ultralight, Three-Dimensional Nanofiber Network. *Chem. Mater.* **2016**, *28*, 8466–8469.

(49) Takeshita, S.; Yoda, S. Upscaled Preparation of Trimethylsilylated Chitosan Aerogel. *Ind. Eng. Chem. Res.* **2018**, *57*, 10421–10430.

(50) Hansen, C. M. ed., *Hansen Solubility Parameters A User's Handbook*, 2nd ed., CRC Press, Boca Raton, 2007.

(51) Ravindra, R.; Krovvidi, K. R.; Khan, A. A. Solubility parameter of chitin and chitosan. *Carbohydr. Polym.* **1998**, *36*, 121–127.

(52) Lehnert, R. J.; Kandelbauer, A. Comments on "Solubility parameter of chitin and chitosan" Carbohydrate Polymers 36 (1998) 121–127. *Carbohydr. Polym.* **2017**, *175*, 601–602.

(53) Zhu, Z.; Snellings, G. M. B. F.; Koebel, M. M.; Malfait, W. J. Superinsulating Polyisocyanate Based Aerogels: A Targeted Search for the Optimum Solvent System. *ACS Appl. Mater. Interfaces* **2017**, *9*, 18222–18230.

(54) Subrahmanyam, R. Gurikov, P.; Dieringer, P.; Sun, M.; Smirnova, I. On the Road to Biopolymer Aerogels—Dealing with the Solvent. *Gels* **2015**, *1*, 291–313.

(55) Liebner, F.; Haimer, E.; Potthast, A.; Loidl, D.; Tschegg, S.; Neouze, M.-A.; Wendland, M.; Rosenau, T. Cellulosic aerogels as ultra-lightweight materials. Part 2 Synthesis and properties. *Holzforschung* **2009**, *63*, 3–11.

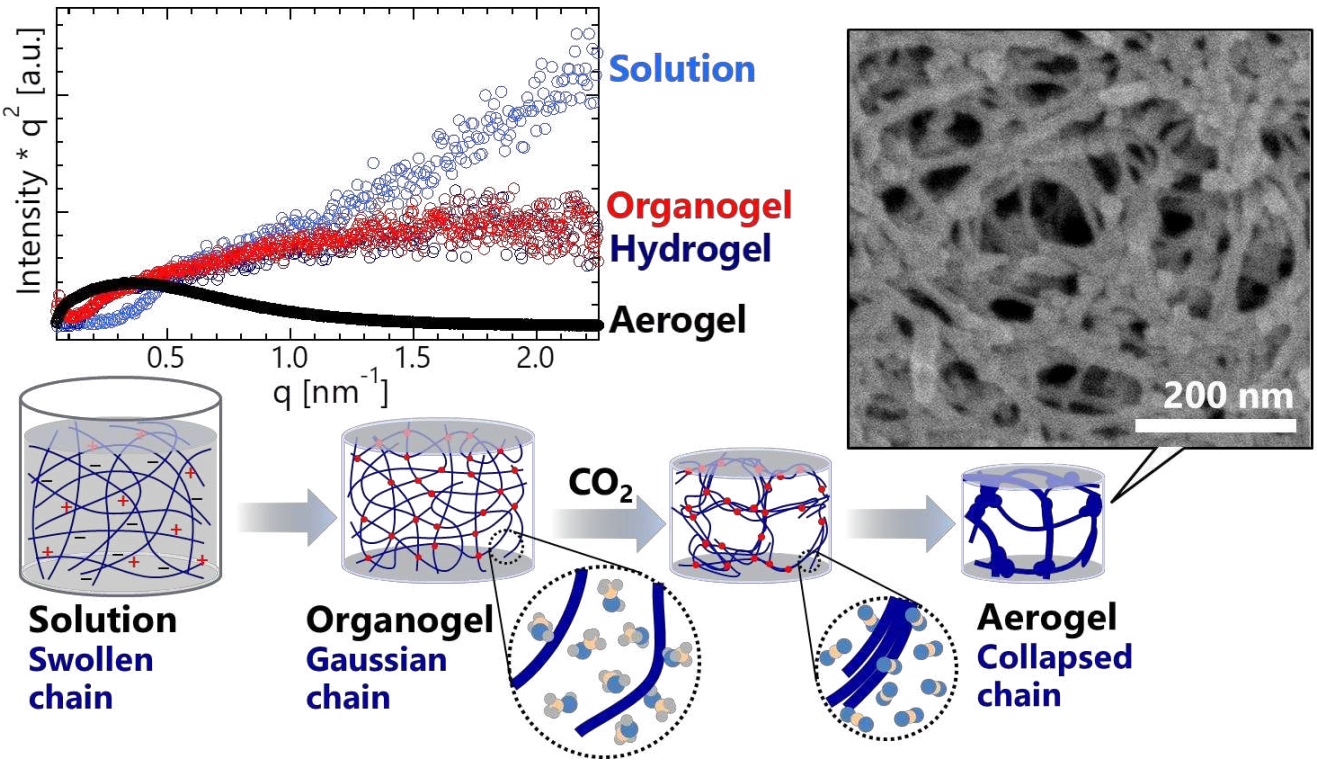

Table of Contents artwork